forests

MDPI

Article

Impacts of Forest-to-Pasture Conversion on Soil Water Retention in the Amazon Biome

Moacir Tuzzin de Moraes [1,2,*], Luiz Henrique Quecine Grande [1,2], Geane Alves de Moura [1], Wanderlei Bieluczyk [3], Dasiel Obregón Alvarez [4], Leandro Fonseca de Souza [5], Siu Mui Tsai [3] and Plínio Barbosa de Camargo [3]

1 Luiz de Queiroz College of Agriculture (ESALQ), University of São Paulo, Piracicaba 13418-900, SP, Brazil; luizquecine@usp.br (L.H.Q.G.); geanealvesm@usp.br (G.A.d.M.)
2 Center for Carbon Research in Tropical Agriculture (CCARBON), University of São Paulo, Piracicaba 13416-823, SP, Brazil
3 Center for Nuclear Energy in Agriculture (CENA), University of São Paulo, Piracicaba 13416-900, SP, Brazil; wanderleibieluczyk@usp.br (W.B.); tsai@cena.usp.br (S.M.T.); pcamargo@cena.usp.br (P.B.d.C.)
4 School of Environmental Sciences, University of Guelph, Guelph, ON N1G 2W1, Canada; dasieloa@uoguelph.ca
5 Center of Agricultural Science and Engineering, Federal University of Espírito Santo, Alegre 29075-910, ES, Brazil; leandro.f.souza@ufes.br
* Correspondence: moacir.tuzzin@usp.br

Abstract

Land-use conversion from forest-to-pasture in the Amazon can affect soil physical quality and hydraulic functioning. The study evaluates the effects of land use (forest and pasture) and soil texture (fine and coarse) on soil structure and hydraulic properties, using the soil water retention curve as an integrative indicator. The study was conducted with soil samples from the Tapajós National Forest region, Pará State, Brazil, with eight sites (four forest and four pasture), balanced by texture. Undisturbed samples were collected from five profile layers (0–10, 10–20, 20–30, and 30–40 cm) for each site, totaling 160 samples. Samples were saturated and measured at soil water matric potentials from −0.1 to −15,000 hPa to obtain the soil water retention curve, which was fitted using the van Genuchten–Mualem model. Pore size distribution was derived from the relationship between soil water matric potential and equivalent pore diameter. Results are reported for the 0–40 cm soil profile (integrating the four sampled layers). Forest-to-pasture conversion altered soil pore structure and water retention in a texture-dependent manner. For fine-textured soils, bulk density increased from 1.03 to 1.31 Mg m^{-3} (+27%) from forest to pasture. In coarse-textured soils, the drainable pore volume up to −15,000 hPa, equivalent diameter > 0.2 μm) decreased from 0.296 to 0.147 m^3 m^{-3} (−50%) from forest to pasture. Plant-available water across the 0–40 cm profile ranged from 0.107 m^3 m^{-3} (pasture, fine-textured) to 0.137 m^3 m^{-3} (forest, coarse-textured). Coarse-textured soils showed a marked reduction in macroporosity, water retention, and plant-available water, whereas fine-texture soils showed smaller changes in water availability but reduced aeration associated with macropore reduction. These results indicate higher physical quality vulnerability of coarse-textured soils following forest-to-pasture conversion.

Keywords: plant-available water; pore size; soil physical quality; soil texture; soil water retention curve

Check for updates

Academic Editor: Carlos R. Mello

Received: 16 December 2025
Revised: 16 January 2026
Accepted: 22 January 2026
Published: 24 January 2026

Copyright: © 2026 by the authors. Licensee MDPI, Basel, Switzerland. This article is an open access article distributed under the terms and conditions of the Creative Commons Attribution (CC BY) license.

1. Introduction

The soil structure influences the main physical processes of water infiltration, redistribution, and storage within the soil profile, with the soil water retention curve serving as a central soil physical quality indicator and hydraulic functioning [1]. The relationship between soil water content and matric potential allows inference of pore-size distribution and hydraulic parameters estimation, such as field capacity and permanent wilting point, which are usually used to estimate the plant-available water content [2]. Changes in soil structure, often associated with soil tillage and compaction, undermine pore space distribution [3] and are directly reflected in soil water dynamics, with implications for water availability to plants [4].

The conversion of tropical forests into pastures and agricultural systems remains one of the major global anthropogenic transformations, driven by the need to increase food production in response to projections of a global population exceeding 9 billion people by 2050 [5]. In this context, Brazil plays a strategic role in global food security [6,7], with a significant portion of its agricultural production associated with the expansion of agropastoral activities into areas originally covered by native vegetation [8], particularly within the Amazon and Cerrado biomes [9,10]. Between 1985 and 2023, Brazil lost more than 110 million hectares of natural vegetation cover, with pasture expansion representing the primary land-use outcome of these converted areas, especially in the Amazon [8], where agricultural activities account for the largest share of recent landscape anthropization [11].

During the conversion process, soils are subjected to mechanical loads associated with machinery traffic and animal trampling, which accelerate structural degradation processes and favor the formation of compacted subsurface layers [12,13]. Soil compaction leads to increased bulk density, reduced microporosity [14], and decreased biological activity [15] associated with the formation and maintenance of soil structure, thereby imposing greater physical resistance to root growth [16]. As a consequence, restrictions to soil permeability, gas diffusion [17], and the availability of water and nutrients to plants are commonly observed, ultimately impairing soil physical functioning [12].

The magnitude and expression of these structural changes are strongly modulated by soil texture. Clayey soils (i.e., fine-textured soils), although exhibiting higher water retention capacity due to the predominance of fine pores, may experience reductions in macroporosity and aeration when subjected to compaction [3], whereas sandy soils, characterized by lower cohesion and structural stability, tend to exhibit more pronounced losses of macropores and mesopores [18]. These texture-dependent differences highlight contrasting vulnerabilities in soil physical quality, with direct implications for degradation risk assessment and for the development of conservation and restoration strategies [19].

Despite advances in characterizing the effects of land-use change on soil physical properties in the Amazon [13] and other tropical [20] and subtropical [21] biomes, contradictions remain in the literature regarding the role of soil texture in modulating changes in porosity and hydraulic behavior following forest-to-pasture conversion [3]. While some studies that analyzed the impacts of land-use changes on soil physical properties over some soil texture indicate greater structural resilience in fine-textured soils [22], others report hydraulic limitations associated with macropore compression [1]. In contrast, in coarse-textured soils (i.e., sandy soils), structural degradation may be rapid and severe even over short periods of use [18]. This heterogeneity of responses indicates that a knowledge gap persists regarding the mechanisms by which soil texture controls pore space reorganization and the resulting changes in hydraulic functions following forest-to-pasture conversion.

Although hydraulic conductivity measurements (e.g., saturated or near-saturated conductivity) are highly informative to quantify infiltration and transmission processes, they are strongly controlled by macropore connectivity [1], exhibit pronounced spatial

and temporal variability in field soils [23], and are highly sensitive to transient boundary conditions. In contrast, the soil water retention curve provides an integrative description of soil water storage across soil water matric potentials [24], allowing mechanistic interpretation of field capacity (−60 hPa) and the permanent wilting point (−15,000 hPa) and their link to plant-available water. Therefore, the soil water retention curve offers a robust and comparable basis to diagnose pore-system reorganization [3] and functional implications of structural degradation after forest-to-pasture conversion across contrasting soil textures.

Despite advances in evaluating land-use change effects on soil physical properties in tropical regions, the extent to which soil texture (especially clay content) controls soil water retention behavior across matric potential ranges after forest-to-pasture conversion in the Amazon biome remains insufficiently resolved, contributing to contradictory interpretations of structural resilience and hydraulic limitation. The novelty of this study is to explicitly quantify how soil texture modulates water retention under forest and pasture land uses in the Amazon and to use soil water retention curves as an integrative basis to infer soil susceptibility to structural degradation. Specifically, this study (i) assesses how soil texture modulates soil water retention under forest versus pasture; (ii) examines the relationship between water retention at different matric potentials and soil clay content in Amazonian soils; and (iii) derives inferences on susceptibility to degradation based on retention-curve behavior as an indicator of pore system reorganization.

Based on this framework, we hypothesize that forest-to-pasture conversion promotes changes in soil physical quality through pore space reorganization, which should be reflected in the soil water retention curve, with contrasting responses between coarse- and fine-textured soils driven by shifts in pore-size classes. Therefore, the objective of this study was to evaluate the effects of land use (forest and pasture) and soil texture (coarse and fine) on soil physical quality, using soil water retention curves as an integrative tool to assess soil structure and hydraulic properties.

2. Materials and Methods

2.1. Study Site and Sampling Design

The study was conducted with soil samples from forest and pasture areas within the Amazon Biome, located in the Tapajós National Forest, Santarém, Pará, Brazil (Figure 1). This region was chosen due to its status as a hotspot for land-use intensification and conversion, particularly driven by livestock expansion over recent decades [25]. The climate is tropical humid (Aw in Köppen classification), with mean annual rainfall of 2000 mm and temperatures around 25 °C. In each site, the primary land-use change sequence occurring in that region, pristine forest to pasture, was evaluated.

The collection of undisturbed soil core samples involved eight sites, which represented four distinct field conditions (Table 1). These conditions were established using a factorial design, considering two primary factors: land use (forest and pasture) and soil texture (coarse and fine). We defined soil texture according to the textural grouping from an average of 0–40 cm depth (Table 1). The particle-size distributions by soil layer (0–10, 10–20, 20–30, and 30–40 cm) are presented in Supplementary Table S1. Two replicate sites were therefore selected for each of the four possible factor combinations, with five individual sampling points chosen within each site (Figure 1). The forest sites were sampled in the Tapajós National Forest in Brazil. The pasture sites were identified in a close region near the National Forest. Forest-to-pasture conversion occurred 15 years ago through a process of selective logging of valuable timber, followed by slash-and-burn deforestation of the remaining vegetation, and finally mechanical seeding of non-native, fast-growing grass *Urochloa* sp. [25].

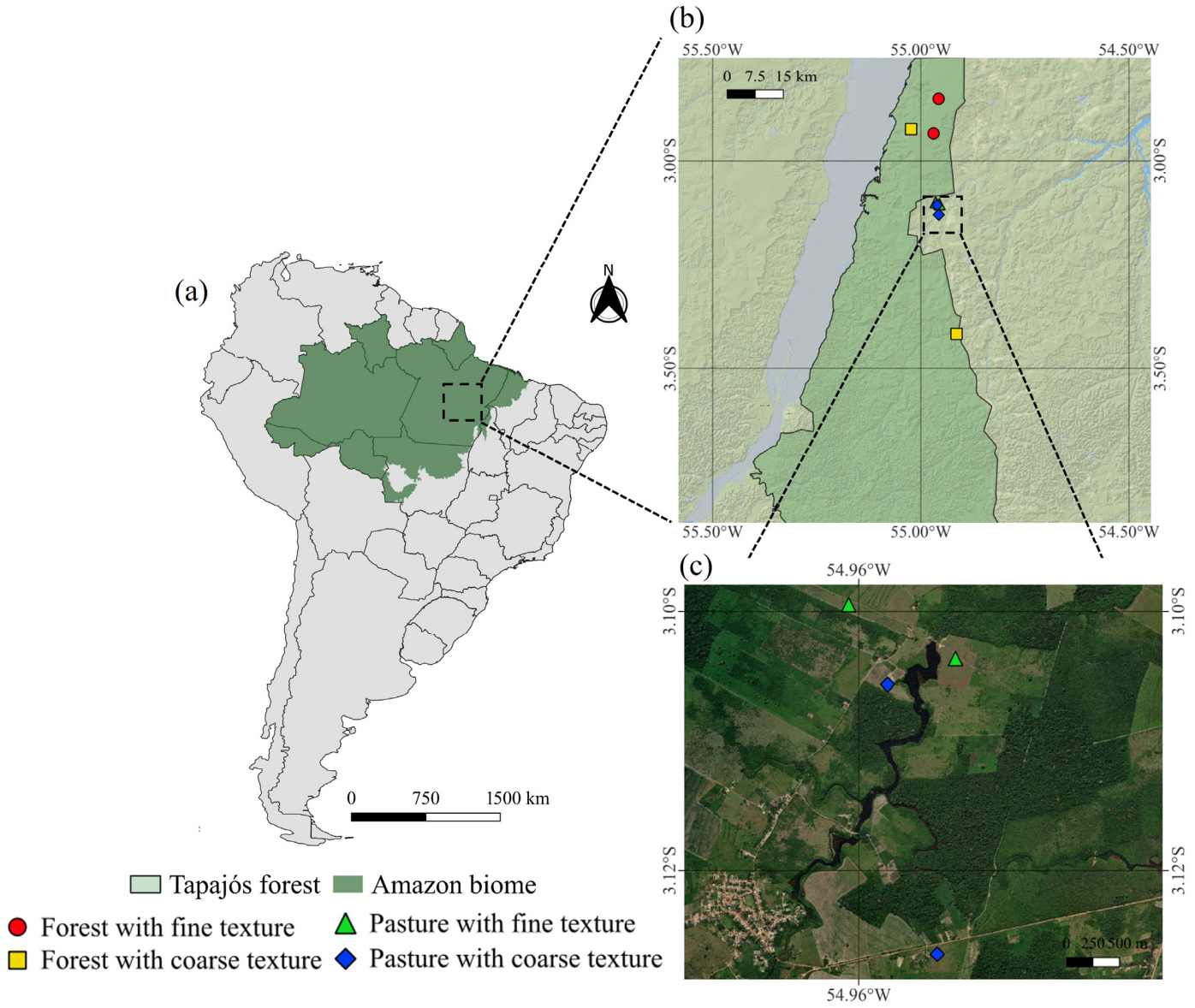


Figure 1. Geographical location of forest and pasture sites in Brazilian Amazon biome: (**a**) South America map highlighting the Amazon biome extent; (**b**) Regional topographic map of the Tapajós National Forest area showing forest (red circles, yellow squares) and pasture (green triangles, blue diamonds) sampling sites with different soil textures; (**c**) High-resolution satellite imagery focusing on pasture areas adjacent to the Tapajós National Forest.

Soil samples with undisturbed structure were collected considering five points (replicates), in a square 100 m × 100 m sampling plot, randomly distributed to capture spatial variability. At each point, intact soil cores were extracted from four depths, i.e., 0–10, 10–20, 20–30, and 30–40 cm. The core samples were sampled with cylindrical metal rings (diameter ≈ 4.7 cm, height ≈ 3.0 cm; volume ≈ 52 cm^3), totalizing 160 samples (8 sites × 4 depths × 5 replicates). Carbon concentration was evaluated by dry combustion in an elemental analyzer (Carlo-Erba, CH-110, Milan, Italy) coupled with an isotope ratio mass spectrometer (IRMS) (Thermo Scientific Delta Plus, Bremen, Germany).

Table 1. Soil carbon content, particle-size distribution (sand, clay, and silt), and textural class for the 0–40 cm soil profile.

Land Use	Texture	Carbon (%)	Sand (g kg^{-1})	Clay (g kg^{-1})	Silt (g kg^{-1})	Textural Class	Soil Class WRB
Forest	Fine	1.76 ± 0.7	14.95 ± 2.0 ^{c}	857.94 ± 11.6 ^{a}	127.11 ± 11.0 ^{a}	Very fine clayey	Ferralsol
Pasture	Fine	1.22 ± 0.7	320.83 ± 64.5 ^{b}	616.34 ± 49.5 ^{b}	62.83 ± 22.0 ^{b}	Very fine clayey	Ferralsol
Forest	Coarse	0.78 ± 0.3	857.24 ± 46.3 ^{a}	79.00 ± 33.8 ^{c}	63.76 ± 21.3 ^{b}	Sandy	Arenosol
Pasture	Coarse	1.04 ± 0.5	627.00 ± 51.5 ^{a}	322.95 ± 52.5 ^{c}	50.05 ± 9.3 ^{b}	Loamy	Ferralsol

Values are observed means ± standard deviation (SD) for the 0–40 cm soil profile, where the 0–40 cm value for each profile was computed as the arithmetic mean of the four 10 cm layers (0–10, 10–20, 20–30, and 30–40 cm). Different superscript letters within each particle-size fraction indicate significant differences among land use × texture combinations (Tukey-adjusted comparisons, $\alpha = 0.05$) based on a linear mixed-effects model fitted by REML (PROC MIXED), with land use, texture, and land use × texture as fixed effects and site nested within land use × texture as a random effect. Textural class grouping was decided according to the Brazilian soil classification system [26]. WRB is the soil classification by the World Reference Base [27].

2.2. Soil Water Retention Analysis

The 160 core samples were prepared in the field to preserve structure and transported to the laboratory. Initial saturation was achieved by capillary rise in deionized water for 24 h. Samples were then subjected to successive soil water matric potentials (h in hPa) using a pressure plate apparatus: −10, −20, −60, −100, −330, −1000, −3000, and −15,000 hPa. The soil water content equivalent to total porosity (equivalent to soil water matric potential of 0.1 hPa) was estimated using the relationship of soil bulk density and particle density (Equation (1)).

$$TP = 1 - \frac{BD}{PD} \quad (1)$$

where TP is total porosity, BD is bulk density and PD is particle density. The soil samples were submitted for each soil water matric potential to ensure hydrostatic equilibrium, after which samples were weighed to determine volumetric water content (θ, m^3 m^{-3}). Dry mass was obtained after oven-drying at 105 °C for 48 h. The Bulk density was calculated as the relationship between the mass and volume of samples.

2.3. Water Retention Curves

Water retention curves were constructed from the measured volumetric soil water content (θ) at each soil water matric potential (h). The 160 individual datasets were fitted to the van Genuchten–Mualem [28] model (Equation (2)) using SWRC software (version 2.00 [29]), which employs nonlinear least-squares optimization to estimate parameters. This resulted in 160 fitted curves, from which means were derived for each depth (0–10, 10–20, 20–30, and 30–40 cm), land use (forest and pasture), and texture (coarse and fine), yielding 16 representative retention curves.

$$\theta = \left(\theta_r + \frac{\theta_s - \theta_r}{\left((1 + \alpha \, | h |)^n \right)^m} \right), \quad (2)$$

where θ is the volumetric water content (m^3 m^{-3}), θ_r and θ_s are residual and saturated water contents (m^3 m^{-3}), respectively, h is the soil water matric potential (hPa), α (hPa^{-1}) is the scale parameter related to the air-entry pressure, n (dimensionless) is the shape parameter reflecting pore-size distribution, and $m = 1 - 1/n$ (following restriction from Mualem [30]) is the tortuosity parameter. Model goodness-of-fit was assessed using the coefficient of determination (R^2).

2.4. Pore Size Distribution Analysis

The pore size distribution by each class was derived from soil water retention curves using the water content between adjacent soil water matric potential thresholds, enabling quantification of each pore class. The equivalent pore diameters were calculated from the reduced form of the capillary rise (Equation (3)) [31]. Pore size distribution was classified into functional classes [31]: macropores (>80 μm), mesopores (30–80 μm), micropores (5–30 μm), ultramicropores (0.1–5 μm), and cryptopores (<0.1 μm). The pore volume associated with pores of equivalent diameter > 0.2 μm (corresponding to −15,000 hPa) was estimated as the difference between total porosity and soil water content at −15,000 hPa.

$$EPD = \frac{3000}{h} \quad (3)$$

where EPD is equivalent pore diameter (μm) and h is soil water matric potential (hPa).

2.5. Statistical Analyses

Soil water retention variables (soil water content at matric potential of −10, −20, −60, −100, −330, −1000, −3000, and −15,000) were evaluated using a 2 × 2 factorial sampling design, with land use (forest vs. pasture) and texture class (fine-textured vs. coarse-textured) as factors. Sampling was stratified by depth (0–10, 10–20, 20–30, and 30–40 cm), with replication within site. For soil water retention variables and other depth-resolved soil attributes, statistical analyses were conducted separately for each depth. For each response variable and depth, data were analyzed using a linear mixed-effects model including land use, texture, and their interaction (land use × texture) as fixed effects and site (*place*) nested within land use × texture as a random effect. Parameters were estimated by restricted maximum likelihood (REML), and fixed-effect tests used the Kenward–Roger method for degrees of freedom. Particle-size fractions (sand, silt, and clay) were measured at each depth but were analyzed using depth-integrated values computed as the arithmetic mean across 0–10, 10–20, 20–30, and 30–40 cm (equal 10 cm layer thickness). The same mixed-model structure (fixed effects: land use, texture, and land use × texture; random effect: site nested within land use × texture) and multiple-comparison procedure were applied to these depth-integrated texture variables. Adjusted means (least-squares means) were obtained for the land use × texture combinations and compared using Tukey-adjusted multiple comparisons. Statistical significance was set at $\alpha = 0.05$. All analyses were performed in SAS (version 9.4, SAS Institute Inc., Cary, NC, USA) using PROC MIXED.

3. Results

Plant water availability is controlled by the energy state of soil water and corresponds to the volume of water retained in soil pores at matric potentials ranging from −60 hPa to −15,000 hPa. The total porosity was higher in fine-textured soils than in coarse-textured soils (Figure 2), with mean values over the 0–40 cm profile of 0.59 m^3 m^{-3} under forest and 0.49 m^3 m^{-3} for pasture. In coarse-textured soils, total porosity ranged from 0.43 under forest to 0.41 m^3 m^{-3} under pasture. Overall, within each textural class, total porosity showed limited variation between forest and pasture along the soil profile.

Soil water retention curves fitted to the van Genuchten–Mualen model showed a high determination coefficient (R^2) (Table 2). The forest-to-pasture conversion impacted changes in soil water retention curves and hence pore size distribution within the soil profile, with more pronounced effects in coarse-textured soils. In these soils, the volume of pores associated with water retention in the 0–40 cm profile decreased from ~0.33 m^3 m^{-3} under forest to 0.17 m^3 m^{-3} under pasture (Figure 2). In fine-textured soils, land-use

conversion also reduced the volume of effective pores for water retention, with mean values decreasing from 0.19 m^3 m^{-3} under forest to 0.14 m^3 m^{-3} under pasture.

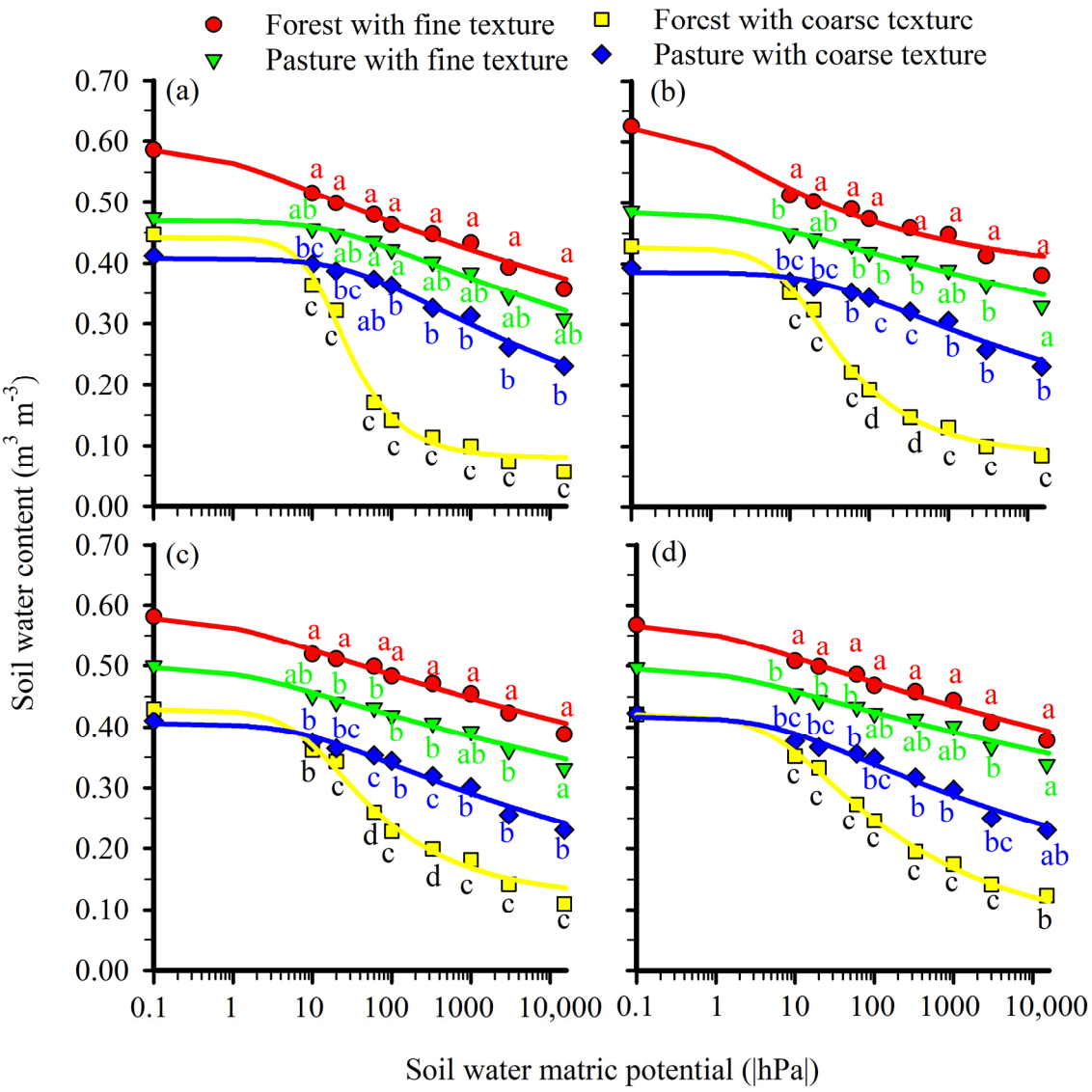


Figure 2. Soil water retention curve for forest and pasture under fine and coarse-textured soils evaluated at 0–10 cm (**a**), 10–20 cm (**b**), 20–30 cm (**c**), and 30–40 cm (**d**) depths. Different letters indicate significant differences among treatments within each soil water matric potential and depth, based on Tukey-adjusted multiple comparisons ($\alpha = 0.05$).

Forest-to-pasture conversion resulted in a marked increase in soil bulk density throughout the profile in fine-textured soils (Figure 3a, Table S2). In coarse-textured soils, bulk density also increased under pasture, particularly at 0–20 cm depth, relative to forest condition (Figure 3a). For the 0–40 cm soil profile, bulk density in fine-textured soils increased from 1.03 Mg m^{-3} under forest to 1.31 Mg m^{-3} under pasture (+0.28 Mg m^{-3}; +27%) (Table S2). In coarse-textured soils, the drainable pore volume up to −15,000 hPa, corresponding to pores with equivalent diameter > 0.2 µm, decreased from 0.296 m^3 m^{-3} under forest to 0.147 m^3 m^{-3} under pasture for the 0–40 cm profile (Table S2). This increase reflected structural changes associated with animal trampling in pasture systems, leading to higher soil compaction and a reduction in the volume of pores larger than 0.2 µm in both texture classes, with porosity values ranging from ~10%–15%. For the 0–40 cm soil profile, plant-available water was highest under forest in coarse-textured soil (0.137 m^3 m^{-3}) and

lowest under pasture in fine-textured soil (0.107 m^3 m^{-3}) (Table S2). This corresponds to an absolute difference of 0.030 m^3 m^{-3} (≈28% higher in forest coarse-textured than in pasture fine-textured).

Table 2. Soil water retention fitted parameters on soil profile (0–40 cm) under forest and pasture conditions in the Amazon Biome.

Site	Texture	SWRC Parameters for van Genuchten–Mualem Equation [1]				
		θ_r	θ_s	α (hPa^{-1})	n	R^2
		---------- 0–10 cm ----------				
Forest	Fine	0.047	0.588	1.5616	1.0498	0.989
Pasture	Fine	0.376	0.626	1.4865	1.1908	0.981
Forest	Coarse	0.070	0.581	1.4707	1.0416	0.986
Pasture	Coarse	0.027	0.569	1.4976	1.0389	0.982
		---------- 10–20 cm ----------				
Forest	Fine	0.010	0.470	0.0553	1.0574	0.982
Pasture	Fine	0.010	0.485	0.5263	1.0374	0.988
Forest	Coarse	0.010	0.498	0.9195	1.0386	0.980
Pasture	Coarse	0.010	0.496	0.8942	1.0353	0.972
		---------- 20–30 cm ----------				
Forest	Fine	0.080	0.442	0.0701	1.8527	0.992
Pasture	Fine	0.086	0.427	0.0918	1.5002	0.995
Forest	Coarse	0.120	0.429	0.1082	1.3961	0.991
Pasture	Coarse	0.057	0.421	0.1510	1.2359	0.997
		---------- 30–40 cm ----------				
Forest	Fine	0.010	0.408	0.0304	1.0929	0.981
Pasture	Fine	0.010	0.386	0.0421	1.0748	0.961
Forest	Coarse	0.010	0.406	0.1332	1.0703	0.964
Pasture	Coarse	0.010	0.417	0.1700	1.0744	0.962

[1] Parameter m is according to van Genuchten–Mualem restriction: $m = 1 - 1/n$. SWRC: Soil water retention curve.

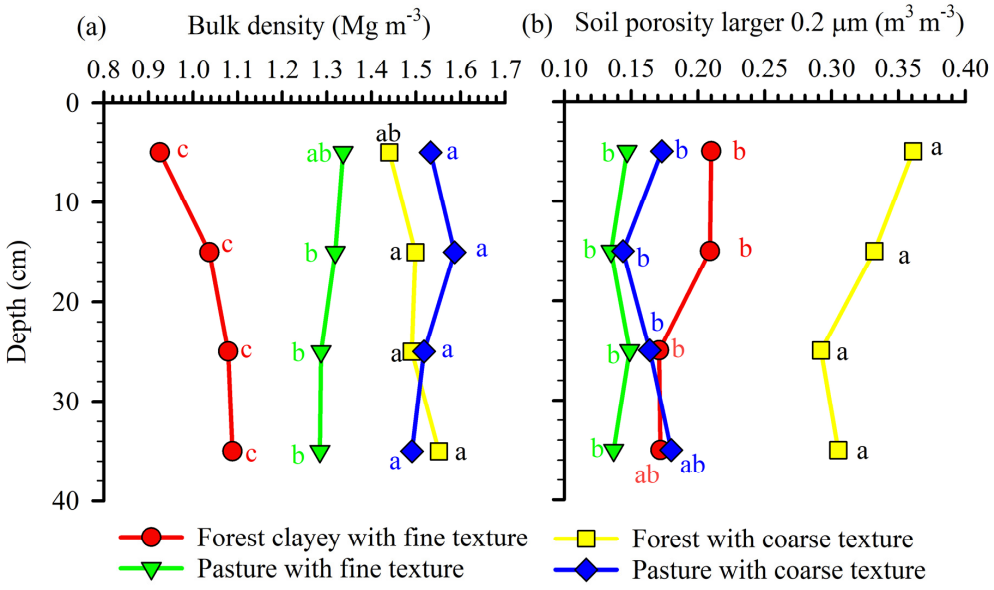


Figure 3. Soil bulk density (**a**) and soil porosity larger than 0.2 µm (**b**) in profile for forest and pasture in fine and coarse-textured soils in Amazon biome. Different letters indicate significant differences among land use × texture combinations within each depth, based on Tukey-adjusted multiple comparisons (α = 0.05).

In response to the replacement of forest by pasture, changes were observed in pore size distribution. Macroporosity (diameter >80 µm) was the most affected pore class, decreasing from 21.4% to 2.5% in the 0–10 cm layer and from 12.7% to 5.5% in the 30–40 cm layer (Figure 4). In clayey soils, these effects were mainly concentrated in the surface layer (0–10 cm), whereas an increase in ultramicropores (pore diameter from 0.1 to 5 µm) occurred in both textural classes, especially to 0–20 cm depth. Changes in mesopores (30–80 µm) and micropores (5–30 µm) across the 0–40 cm profile were observed only in coarse-textured soils.

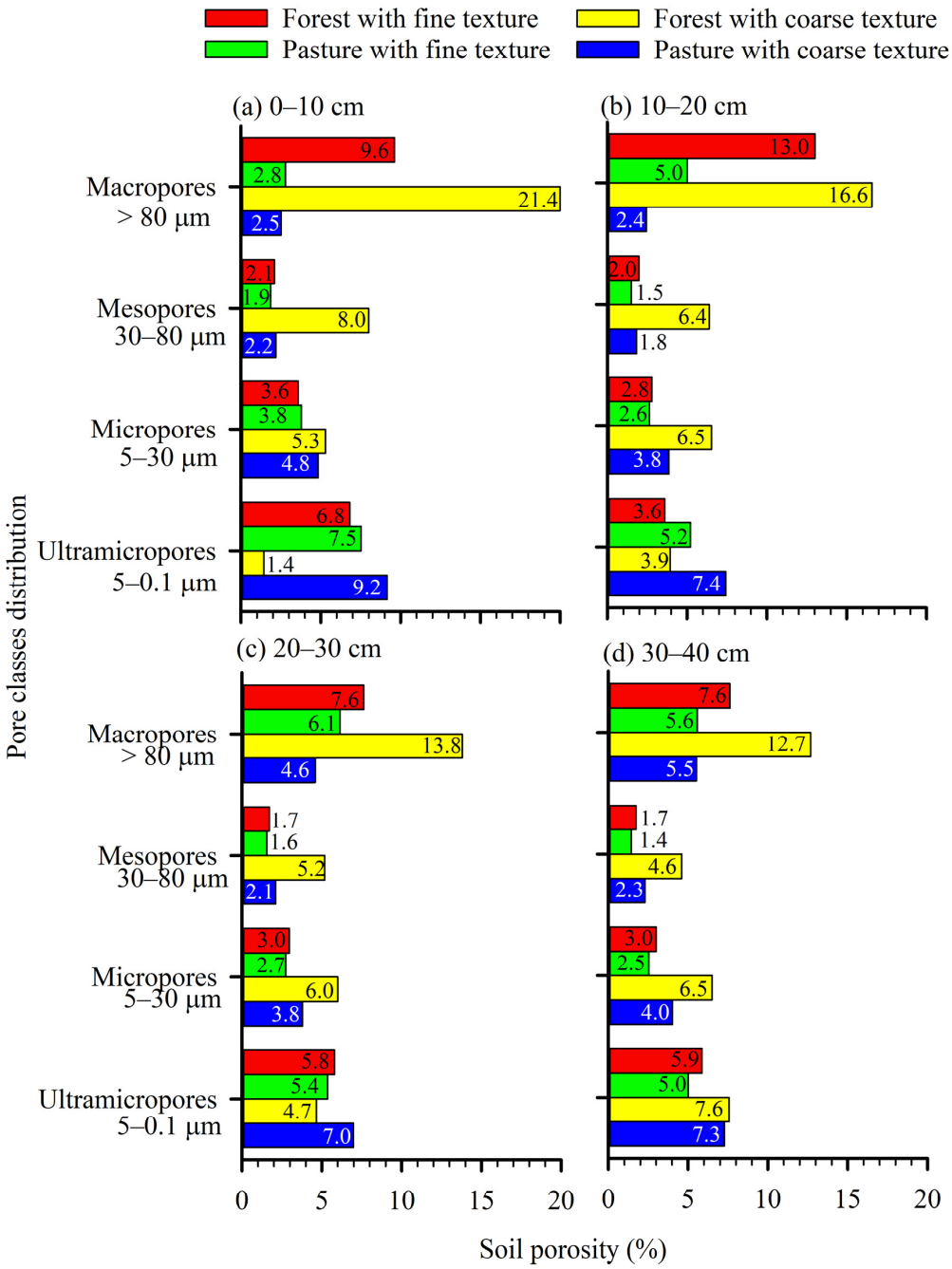


Figure 4. Pore distribution by pore size classes according to category of microporosity, mesoporosity, microporosity, and ultramicroposity under forest and pasture for fine and coarse-textured soils in Amazon biome evaluated at 0–10 cm (**a**), 10–20 cm (**b**), 20–30 cm (**c**), and 30–40 cm (**d**) depths. No statistical analysis is shown because these values were derived from the soil water retention curve data presented in Figure 2.

Soil water content at field capacity and at the permanent wilting point differed between forest and pasture (Figures 5a and 6), with smaller changes in fine-textured soils than coarse-textured soils. Plant available water, expressed as the differences between these two hydraulic states (Figure 5b), was reduced under pasture, particularly in the deeper soil layers (20–40 cm), compared with the forest condition (Figure 5b). When we compare the soil water content over a large range of clay content, the water content is very different between fine and coarse-textured soils. To understand the effects of water in the soil, we need to compare the treatments under the same energy for water retention; thus, for all soil textures, the water available (average in soil profile of 0–40 cm depth) ranged from 0.086 m^3 m^{-3} for fine-textured soils to ~0.123 m^3 m^{-3} for coarse-textured soils. In addition, the subsoil layers of 20–40 cm depth showed lower available water in coarse-textured soil under pasture (0.11 m^3 m^{-3}) than coarse-textured soil with forest (0.14 m^3 m^{-3}).

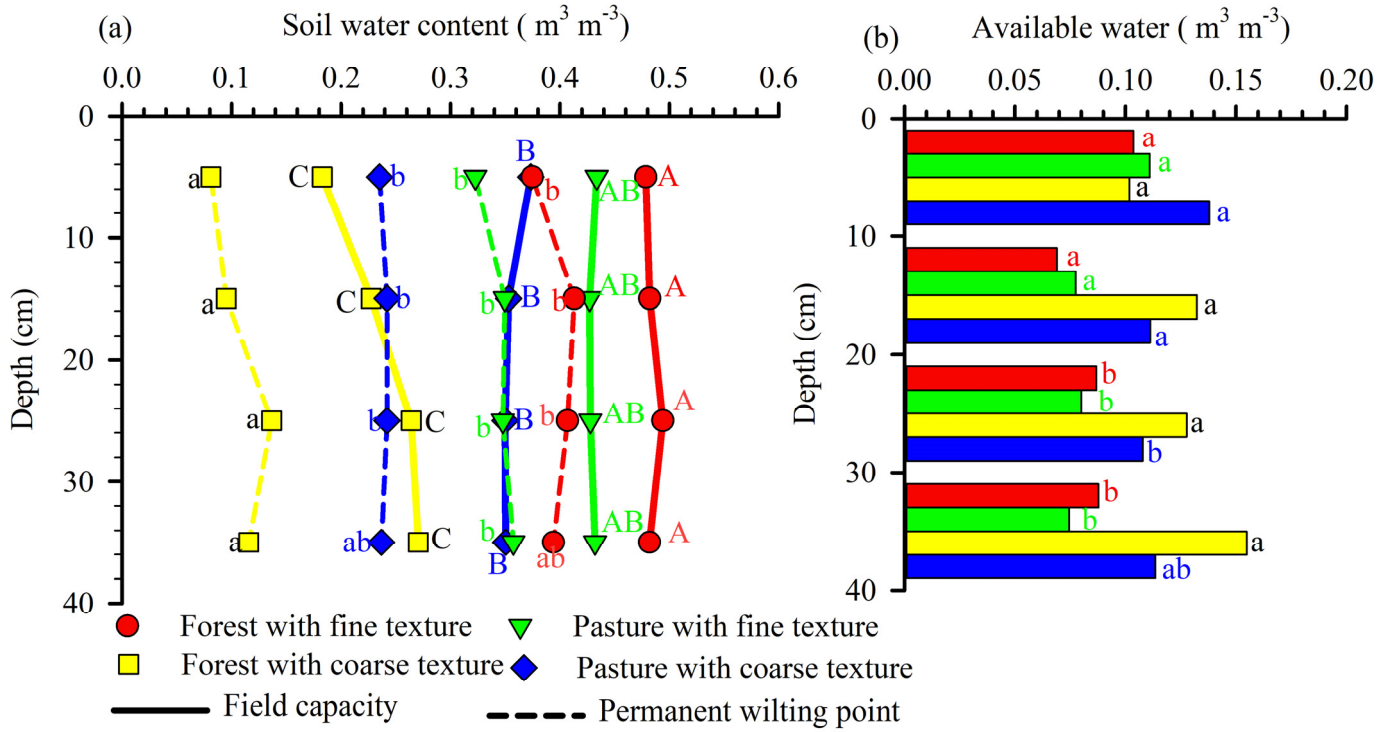


Figure 5. Soil water content at field capacity (soil water matric potential of −60 hPa, solid lines) and permanent wilting point (−15,000 hPa, dashed lines) (**a**) and plant available water (**b**) for forest and pasture condition for fine and coarse-textured soils in Amazon biome. Symbols represent land use and texture combinations: forest fine (red circles), forest coarse (yellow squares), pasture fine (green triangles), and pasture coarse (blue diamonds). Different letters indicate significant differences among land use × texture combinations within each depth, based on Tukey-adjusted multiple comparisons ($\alpha = 0.05$).

The soil water retention presented a relationship with clay content (Figure 6), and it showed that, when forest and pasture samples are pooled, clay content strongly increases water retention at both field capacity (−60 hPa) and the permanent wilting point (−15,000 hPa). Soil water retention in volumetric content (Figure 6a) and gravimetric content (Figure 6b) can be used as a driver to understand how that clay content changes the water retention over field capacity and permanent wilting point. In addition, we could estimate that water retention using that clay content for soils in Amazon biome. This pattern clarifies why higher total retention in finer-textured soils does not necessarily lead to higher plant-available water. A considerable fraction of the additional water retained with increasing clay is held at very low matric potentials (closer to −15,000 hPa) and is

therefore not plant-extractable. In contrast, sandy soils retain less water overall but retain much less at the permanent wilting point, which can yield a relatively larger and higher average available water.

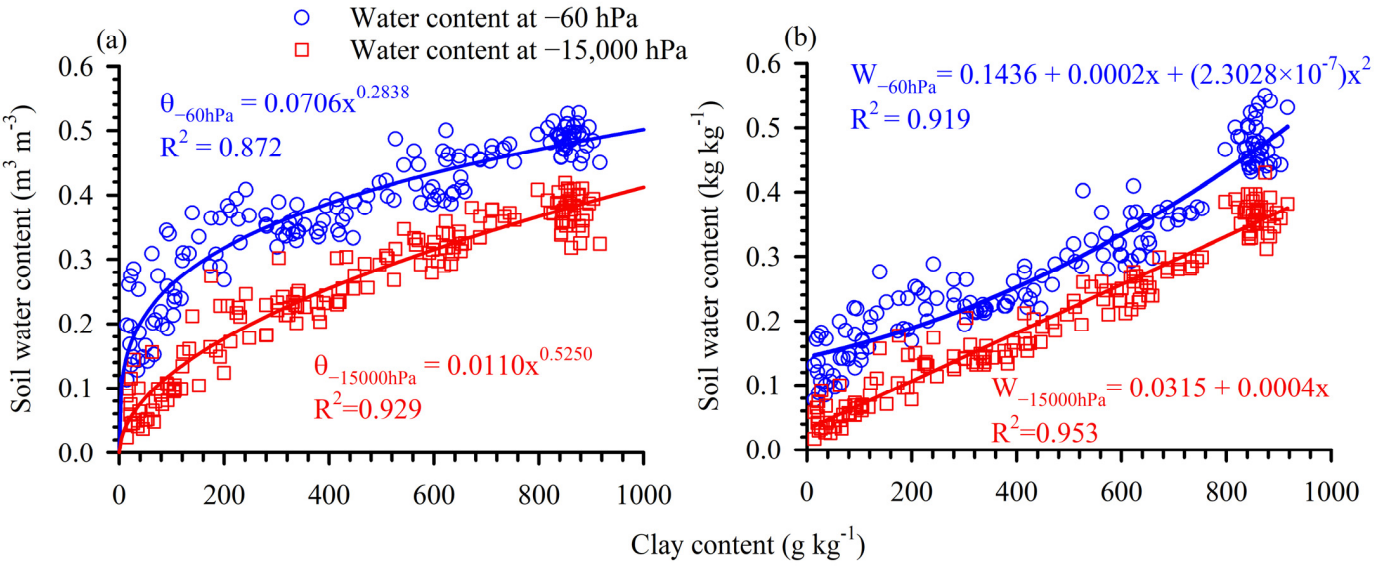


Figure 6. Relationship of clay content with volumetric (**a**) and gravimetric (**b**) soil water content at field capacity (soil water matric potential of −60 hPa) and permanent wilting point (−15,000 hPa) for soils under forest and pasture in Amazon Biome. θ volumetric soil water content (m^3 m^{-3}); W gravimetric soil water content (kg kg^{-1}).

4. Discussion

Water availability to plants is fundamentally regulated by soil structure, particularly by pore arrangement, which affects the soil water energy status and flux. Our study highlighted the texture-driven impact of land-use change on soil pore space and hydraulic functions. The forest-to-pasture conversion resulted in soil structure degradation, expressed by a reduction in total porosity, most notably macroporosity and mesoporosity, and in soil water availability. Mechanistically, this pattern indicates a preferential loss of the structural pore domain (inter-aggregate pores and biopores) rather than the textural (matrix) porosity. Forest soils typically maintain a connected macropore network through continuous root turnover and bioturbation, which stabilizes inter-aggregate voids and promotes pore continuity. After conversion to pasture, repeated mechanical stresses (tillage, machinery traffic, and/or livestock trampling) promote particle rearrangement, pore necking, and collapse of transmission pores, reducing not only the volume of macro- and mesopores but also their connectivity, with direct consequences for infiltration, aeration, and root exploration. Soares et al. [13], studying the impact of land use and occupation on physical properties in the Amazon, reported a macroporosity decrease, associated with a bulk density and soil penetration resistance increase, supporting our findings. Despite the empirical approach used to assess the variability of water availability across land uses and soil textures, our study was able to identify fundamental changes in soil physical quality, with a pronounced influence of soil texture across land-use types, which was possible by the high-resolution soil water retention curve, strongly associated with soil structure and key hydraulic functions. Some studies have shown the detrimental impact of forest-to-pasture conversion [32,33] on soil physical properties and soil quality, but the influence of soil texture on the main physical alterations remains overlooked and unclear. These texture-driven differences highlight the distinct vulnerability of soils regarding physical

quality, underscoring its importance for decision-makers, especially in soil degradation risk assessments as well as in strategies for soil quality conservation and restoration.

The forest-to-pasture conversion altered the pore space arrangement differently in coarse and fine-textured soils, most likely reflecting differences in pore connectivity and aggregate stability. Sandy soils are often more vulnerable to structural degradation because they exhibit lower aggregate stability and weaker inter-particle bonding, making their pore system more dependent on biological structuring and organic binding agents. Under comparable mechanical loads, this results in a proportionally larger collapse of macro- and mesopores, with stronger impacts on the plant-available water range. In coarse-textured soils, the reduction in volumetric water content at slightly negative matric potentials (i.e., from –1 to –100 hPa) suggests a decrease in the volume of macropores and mesopores, mainly due to compaction processes [34]. Because this suction interval is largely controlled by transmission and storage pores close to field capacity, the observed shift implies a reduction in soil water content near field capacity, which mechanistically explains the decline in plant-available water.

We estimated water retention at field capacity (−60 hPa) and at the permanent wilting point (−15,000 hPa) across the observed range of clay contents on a volumetric basis (Figure 6a) and a gravimetric basis (Figure 6b). Our pedotransfer can be used to estimate soil water content under field conditions, particularly when expressed on a mass basis (Figure 6b), which is often more directly comparable across soils with contrasting bulk densities. Water retention near −60 hPa is predominantly governed by structural pores (macro- and mesopores and their connectivity) and is therefore highly sensitive to land-use-induced changes in aggregation, pore continuity, and compaction, whereas retention at −15,000 hPa is largely controlled by textural (matrix) porosity, being strongly associated with clay content and specific surface area and less directly affected by collapse of transmission pores. Consequently, increasing clay content tends to raise retention at both potentials (Figure 6), but the increment at −15,000 hPa represents water that is mostly non-extractable by plants, helping to explain why higher total retention does not necessarily translate into higher plant-available water. In this context, Utin et al. [35] showed that time variability in soil water retention curve can be inferred using only bulk density, saturated water content, and macroporosity, emphasizing that structural indicators, particularly those linked to the pore domain controlling retention close to field capacity, provide a practical basis to track and interpret changes in soil water retention induced by management and structural dynamics.

Thus, higher total retention in clayey soils does not necessarily translate into higher plant-available water because a larger proportion is retained in small pores at potentials below the plant-extractable range. In line with this, Van Lier [36] reported no significant correlation between flux-based total and readily available water with clay content in tropical soils, suggesting that texture alone may not predict plant-available water when water availability is evaluated from a flux perspective. This apparent discrepancy can be explained by differences in the conceptual definition of water availability (retention-based vs. flux-based), and by the additional control of soil structure, pore connectivity, and compaction on water supply to roots.

Under forest cover, the continuous root activity, plant diversity, and macrofaunal activity contribute to the formation and maintenance of macropores and, particularly, biopores [37]. Replacement by pasture exposes the soil to recurrent mechanical stresses (tillage, machinery traffic, and/or trampling), which promote compaction and pore network reorganization, leading to losses in structural pores and reduced pore continuity [38]. These soil disturbance and compaction processes are expressed by decreased water permeability [12], reduced gas diffusivity [17], and increased mechanical impedance to root growth [14]. Similar effects have been reported in the Amazon, with a drastic reduction

in infiltration and saturated hydraulic conductivity (from 1258 mm h^{-1} to 100 mm h^{-1}) following conversion [39].

The reduction in total porosity observed in the fine-textured soil after conversion to pasture, together with the increase in bulk density across the studied layers, highlights the negative impact of this land-use change. Although no significant increase in bulk density was detected in the coarse-textured soil following conversion, a pronounced reduction in the proportion of larger-diameter pores (i.e., macropores and mesopores) was verified in all layers, resulting in a drastic alteration of soil structure and hydraulic functions (i.e., water availability), according to Owuor et al. [40], who also reported a decreased water availability and infiltration after land-use change. This alteration is explained by the greater susceptibility of coarse-textured soils to compaction due to their lower load-bearing capacity. In addition, sandy soils exhibit low structural stability, even over short temporal scales [18], which supports the marked structural degradation observed after pasture establishment. Therefore, the vulnerability of soil physical quality and functions to land cover and management systems is inherently influenced by soil texture, and understanding these relationships is essential for maintaining the sustainability of agricultural systems, particularly under conditions of greater water deficit, in which soil hydraulic properties play a fundamental role [41].

In a long-term study, Kooch et al. [20] identified a reduction in soil health following forest-to-pasture conversion, characterized by decreased organic matter content, reduced phosphorus and nitrogen levels, diminished aggregate stability, increased bulk density, and a reduction in pore space. In other hand, livestock–forestry integration systems (LFI) have been employed to maintain soil structure and hydraulic properties, as well as to recover degraded areas [42]. Moreover, Nascimento et al. [43] reported that system intensification by crop–livestock integration (CLI) enhanced water infiltration, soil aeration capacity, water availability, and reduced the degree of soil compactness. The intensification of cropping systems combined with conservationist practices (i.e., no-tillage) promotes continuous root activity, contributing to the formation and maintenance of pore space [44], which in turn improves soil physical properties [45]. Additionally, over time, conservationist systems increase soil resistance to compaction due to the formation and strengthening of cohesion bonds between particles [46,47]. These strategies are particularly crucial concerning soil texture, as coarse-textured soils' physical quality exhibits greater vulnerability when subjected to land-cover and land-use changes.

Soil structure plays an essential role in determining the physical processes, such as water flow [1], gas diffusivity [48], as well as providing low-resistance pathways for root elongation [49]. The soil structure and hence its physical functions is one of the main factors governing the plant growth environment within the soil–plant–atmosphere system [50], reinforcing the importance of understanding the impacts of land-use conversion on soil physical quality, particularly under contrasting textural scenarios. Accordingly, our study was able to identify these impacts throughout the soil surface layers and, particularly, to highlight differences in behavior and vulnerability between fine and coarse-textured soils regarding structural degradation, with a pronounced water availability decrease in coarse-textured soils. Although the effects of these alterations on hydraulic permeability (i.e., infiltration and hydraulic conductivity) were not evaluated, we comprehensively assessed the impacts on soil structure, particularly on pore space, and on soil water retention capacity. This information is essential for emphasizing the relevance of conservationist systems, integrated cropping systems, and soil degradation risk assessments.

5. Conclusions

A comprehensive study of soil structure was performed, based on the high-detailed water retention curve, to assess the impact of forest-to-pasture conversion on the physical quality under fine and coarse-textured soils. The conversion implied a decrease in macropore and mesopore volume across the soil profile, markedly in the coarse-textured soils, in which a pronounced water availability decrease was observed. To mitigate hydrological degradation after forest-to-pasture conversion, particularly in sandy soil, we recommend traffic/trampling control, continuous soil cover, and organic matter inputs to promote aggregate stability and biopore formation by soil structure preservation with a no-tillage system. Coarse-textured soils are particularly fragile, and forest-to-pasture conversion can rapidly degrade soil structure; therefore, these areas should preferably be conserved under forest cover. The texture-driven impacts of forest-to-pasture conversion highlight the greater physical quality vulnerability of coarse-textured soils adopting well-managed, biodiverse integrated livestock systems, preferably incorporating regionally adapted tree components, to protect the soil and promote soil physical multifunctionality. Overall, our results show that soil texture controls how forest-to-pasture conversion alters the soil water retention curve and plant-available water. This soil water retention curve–based framework provides a basis for future studies to track degradation/recovery and support modelling of land-use impacts in tropical soils.

Supplementary Materials: The following supporting information can be downloaded at: https://www.mdpi.com/article/10.3390/f17020157/s1, Table S1: Characterization of the soil particle distribution and textural grouping in layers of soil profile; Table S2: Bulk density, pore larger 0.2 μm and available water for the 0–40 cm soil profile in Amazon Biome.

Author Contributions: Conceptualization, M.T.d.M.; methodology, M.T.d.M.; software, M.T.d.M. and L.H.Q.G.; formal analysis, M.T.d.M.; investigation, M.T.d.M., W.B., D.O.A., L.F.d.S. and P.B.d.C.; data curation, M.T.d.M.; writing—original draft preparation, M.T.d.M., L.H.Q.G., and G.A.d.M.; writing—review and editing, M.T.d.M., L.H.Q.G. and G.A.d.M.; supervision, M.T.d.M.; funding acquisition, M.T.d.M., S.M.T. and P.B.d.C. All authors have read and agreed to the published version of the manuscript.

Funding: The authors are grateful to São Paulo Research Foundation (FAPESP), which supported the research (grant no. 2014/50320-4) and provided scholarships to M.T.d.M. (grant no. 2017/11332-5), L.H.Q.G. (grant no. 2024/05953-0 and 2025/27150-0), W.B. (2019/11806-2 and 2023/18333-8), D.O.A. (grant no. 2016/24695-6 and 2018/05223-1), and L.F.d.S. (2018/09117-1).

Data Availability Statement: The original contributions presented in this study are included in the article, and further inquiries can be directed to the corresponding author.

Conflicts of Interest: The authors declare no conflicts of interest.

References

1. Grande, L.H.Q.; da Silva, L.H.A.; dos Santos, J.K.; de Alencar, A.A.; Pereira, M.B.N.; Macedo, M.D.; Soltangheisi, A.; Ruiz, F.F.; Bolonhezi, D.; de Moraes, M.T. Soil Hydraulic Functions in a Long-Term Conservation Tillage System for Sugarcane. *Soil Tillage Res.* **2026**, *256*, 106908. [CrossRef]
2. de Jong van Lier, Q.; de Melo, M.L.A.; Pinheiro, E.A.R. Stochastic Analysis of Plant Available Water Estimates and Soil Water Balance Components Simulated by a Hydrological Model. *Vadose Zone J.* **2024**, *23*, e20306. [CrossRef]
3. Talat, A.E.; Wang, J.; El-Sorogy, A.S. Impact of Soil Compaction on Pore Characteristics and Hydraulic Properties by Using X-Ray CT and Soil Water Retention Curve in China's Loess Plateau. *Water* **2025**, *17*, 1144. [CrossRef]
4. Jarvis, N.; Coucheney, E.; Lewan, E.; Klöffel, T.; Meurer, K.H.E.; Keller, T.; Larsbo, M. Interactions between Soil Structure Dynamics, Hydrological Processes, and Organic Matter Cycling: A New Soil-crop Model. *Eur. J. Soil Sci.* **2024**, *75*, e13455. [CrossRef]

5. FAO. *The State of Food and Agriculture 2023—Revealing the True Cost of Food to Transform Agrifood Systems*; FAO: Rome, Italy, 2023. [CrossRef]
6. Gomes, V.H.F.; Andrino, C.O.; Barbosa-Silva, R.G.; Acosta, A.L.; González-Chaves, A.D.; Slätis, J.; Giannini, T.C. Food Insecurity under Global Human-Induced Changes: Plants of the Future in the Amazonian Biome. *Biol. Conserv.* **2025**, *311*, 111398. [CrossRef]
7. FAO; IFAD; UNICEF; WFP; WHO. *The State of Food Security and Nutrition in the World 2025*; FAO: Rome, Italy; IFAD: Rome, Italy; UNICEF: New York, NY, USA; WFP: Rome, Italy; WHO: Geneva, Switzerland, 2025. [CrossRef]
8. Caballero, C.B.; Biggs, T.W.; Vergopolan, N.; West, T.A.P.; Ruhoff, A. Transformation of Brazil's Biomes: The Dynamics and Fate of Agriculture and Pasture Expansion into Native Vegetation. *Sci. Total Environ.* **2023**, *896*, 166323. [CrossRef]
9. Flores, B.M.; Montoya, E.; Sakschewski, B.; Nascimento, N.; Staal, A.; Betts, R.A.; Levis, C.; Lapola, D.M.; Esquível-Muelbert, A.; Jakovac, C.; et al. Critical Transitions in the Amazon Forest System. *Nature* **2024**, *626*, 555–564. [CrossRef]
10. Haddad, E.A.; Araújo, I.F.; Feltran-Barbieri, R.; Perobelli, F.S.; Rocha, A.; Sass, K.S.; Nobre, C.A. Economic Drivers of Deforestation in the Brazilian Legal Amazon. *Nat. Sustain.* **2024**, *7*, 1141–1148. [CrossRef]
11. Obregon Alvarez, D.; Fonseca de Souza, L.; Mendes, L.W.; de Moraes, M.T.; Tosi, M.; Venturini, A.M.; Meyer, K.M.; Barbosa de Camargo, P.; Bohannan, B.J.M.; Mazza Rodrigues, J.L.; et al. Shifts in Functional Traits and Interactions Patterns of Soil Methane-cycling Communities Following Forest-to-pasture Conversion in the Amazon Basin. *Mol. Ecol.* **2023**, *32*, 3257–3275. [CrossRef]
12. da Silva, T.S.; Suzuki, L.E.A.S.; Tormena, C.A.; Schmidt, M.R.; Mazurana, M.; Levien, R. Soil Tillage and Cropping System Effects on the Physical-Hydric Properties of a Soil under No-Tillage. *Sustainability* **2023**, *15*, 15936. [CrossRef]
13. Soares, M.D.R.; de Souza, Z.M.; Campos, M.C.C.; da Silva, R.B.; Esteban, D.A.A.; Noronha, R.L.; dos Santos Gomes, M.G.; da Cunha, J.M. Land-Use Change and Its Impact on Physical and Mechanical Properties of Archaeological Black Earth in the Amazon Rainforest. *Catena* **2021**, *202*, 105266. [CrossRef]
14. Marques Filho, A.C.; Martins, M.B.; Santana, L.S.; Lopes, A.G.C.; Sobrinho, R.L.; Souza, E.F.C.; Okla, M.K.; Alaraidh, I.A. Effect of Soil Compaction Caused by Manual and Mechanized Harvesting Management on Sugarcane Yield. *Sugar Tech* **2025**, *27*, 1351–1361. [CrossRef]
15. Uchôa, S.C.P.; Pereira, L.F.; de Matos, C.H.L.; do Nascimento Tavares, I.; Alves, J.M.A.; do Vale Júnior, J.F. Impact of Forest Conversion to Pasture on Soil Enzymatic Activity in the Northern Amazon. *Rev. Agric. Neotrop.* **2024**, *11*, e8585. [CrossRef]
16. de Moraes, M.T.; Olbermann, F.J.R.; de Andrade Bonett, J.; Pilegi, L.R.; Costa, M.V.R.; Pacheco, V.; Rogers, C.D.; Guimarães, R.M.L. The Impacts of Cover Crop Mixes on the Penetration Resistance Model of an Oxisol under No-Tillage. *Soil Tillage Res.* **2024**, *242*, 106138. [CrossRef]
17. Fu, Z.; Yan, Z.; Li, S. Effects of Soil Pore Structure on Gas Diffusivity under Different Land Uses: Characterization and Modelling. *Soil Tillage Res.* **2024**, *237*, 105988. [CrossRef]
18. Phalempin, M.; Jentzsch, N.; Köhne, J.M.; Schreiter, S.; Gründling, R.; Vetterlein, D.; Schlüter, S. Soil Structure Development in a Five-Year Chronosequence of Maize Cropping on Two Contrasting Soil Textures. *Soil Tillage Res.* **2025**, *251*, 106561. [CrossRef]
19. Kooch, Y.; Kartalaei, Z.M.; Amiri, M.; Zarafshar, M.; Shabani, S.; Mohammady, M. Soil Health Reduction Following the Conversion of Primary Vegetation Covers in a Semi-Arid Environment. *Sci. Total Environ.* **2024**, *921*, 171113. [CrossRef]
20. Mello, C.R.; Guzman, J.A.; Vieira, N.P.A.; Viola, M.R.; Beskow, S.; Guo, L.; Alvarenga, L.A.; Rodrigues, A.F. Mitigating Severe Hydrological Droughts in the Brazilian Tropical High-Land Region: A Novel Land Use Strategy under Climate Change. *Int. Soil Water Conserv. Res.* **2025**, *13*, 627–643. [CrossRef]
21. Costa, A.G.; Soares, M.F.; Guevara, M.F.; Nunes, R.F.; da Silva, D.M.; Armindo, R.A.; Timm, L.C. Land-Use Effects on Soil Physical Quality: A Watershed-Scale Hierarchical Assessment. *Catena* **2025**, *261*, 109552. [CrossRef]
22. de Andrade Bonetti, J.; Anghinoni, I.; Bredemeier, C.; Moraes, M.T.; Tormena, C.A.; Gubiani, P.I. Physical Recovery of an Oxisol under an Integrated Crop-Livestock System in Southern Brazil. *Arch. Agron. Soil Sci.* **2023**, *69*, 507–518. [CrossRef]
23. Wu, X.; Yang, Y.; He, T.; Wang, Y.; Liu, B.; Liu, Y. Temporal Variability of Saturated Hydraulic Conductivity on a Typical Black Soil Slope of Northeast China. *Catena* **2024**, *236*, 107742. [CrossRef]
24. Huf dos Reis, A.M.; Pires, L.F.; Armindo, R.A. New Empirical-Point Pedotransfer Functions for Water Retention Data for a Wide Range of Soil Texture and Climates. *Int. Soil Water Conserv. Res.* **2024**, *12*, 855–867. [CrossRef]
25. Soltangheisi, A.; Moraes, M.T.; Cherubin, M.R.; Alvarez, D.O.; de Souza, L.F.; Bieluczyk, W.; Navroski, D.; Bettoni Teles, A.P.; Pavinato, P.S.; Martinelli, L.A.; et al. Forest Conversion to Pasture Affects Soil Phosphorus Dynamics and Nutritional Status in Brazilian Amazon. *Soil Tillage Res.* **2019**, *194*, 104330. [CrossRef]
26. Dos Santos, H.G.; Jacomine, P.K.T.; dos Anjos, L.H.C.; de Oliveira, V.A.; Lumbreras, J.F.; Coelho, M.R.; de Almeida, J.A.; de Araujo Filho, J.C.; de Oliveira, J.B.; Cunha, T.J.F. *Brazilian Soil Classification System*, 5th ed.; Reichart, C.E.A., dos Anjos, L.H.C., Alves, M.D.C., dos Santos, H.G., Lumbreras, J.F., Eds.; Embrapa Soils (CNPS): Brasília, Brazil; Embrapa: Brasília, Brazil, 2018; ISBN 978-85-7035-821-9.
27. IUSS Working Group WRB. *World Reference Base for Soil Resources. International Soil Classification System for Naming Soils and Creating Legends for Soil Maps*, 4th ed.; International Union of Soil Sciences (IUSS): Vienna, Austria, 2022; ISBN 979-8-9862451-1-9.

28. van Genuchten, M.T. A Closed-Form Equation for Predicting the Hydraulic Conductivity of Unsaturated Soils. *Soil Sci. Soc. Am. J.* **1980**, *44*, 892–898. [CrossRef]
29. Dourado-Neto, D.; Nielsen, D.R.; Hopmans, J.W.; Reichardt, K.; Bacchi, O.O.S. Software to Model Soil Water Retention Curves (SWRC, Version 2.00). *Sci. Agric.* **2000**, *57*, 191–192. [CrossRef]
30. Mualem, Y. A New Model for Predicting the Hydraulic Conductivity of Unsaturated Porous Media. *Water Resour. Res.* **1976**, *12*, 513–522. [CrossRef]
31. Weil, R.R..; Brady, N.C. *The Nature and Properties of Soils*, 15th ed.; Weil, R.R., Brady, N.C., Eds.; Pearson: Upper Saddle River, NJ, USA, 2017; ISBN 978-0133254488.
32. Oliveira, S.P.; Cândido, M.J.D.; Weber, O.B.; Xavier, F.A.S.; Ortiz Escobar, M.E.; Oliveira, T.S. Conversion of Forest into Irrigated Pasture II. Changes in the Physical Properties of the Soil. *Catena* **2016**, *143*, 70–77. [CrossRef]
33. Cherubin, M.R.; Chavarro-Bermeo, J.P.; Silva-Olaya, A.M. Agroforestry Systems Improve Soil Physical Quality in Northwestern Colombian Amazon. *Agrofor. Syst.* **2019**, *93*, 1741–1753. [CrossRef]
34. Martínez, I.; Stettler, M.; Lorenz, M.; Brunotte, J.; Weisskopf, P.; Sommer, M.; Keller, T. Immediate Effects of Wheeling with Agricultural Machinery on Topsoil Gas Transport Properties and Their Anisotropy. *Soil Tillage Res.* **2024**, *241*, 106126. [CrossRef]
35. Utin, U.E.; Geris, J.; Smith, J.U.; Hallett, P.D. Using Only Bulk Density, Saturated Water Content and Macroporosity Measurements to Infer Time Variability in Soil Water Retention Curves. *Soil Tillage Res.* **2026**, *257*, 106990. [CrossRef]
36. de Jong van Lier, Q. Flux-Based Plant Water Availability in Tropical Soils from Brazil. *Discov. Soil* **2025**, *2*, 39. [CrossRef]
37. Xiong, P.; Zhang, Z.; Peng, X. Root and Root-Derived Biopore Interactions in Soils: A Review. *J. Plant Nutr. Soil Sci.* **2022**, *185*, 643–655. [CrossRef]
38. Mooney, S.J.; Young, I.M.; Heck, R.J.; Peth, S. X-Ray Imaging of Mechanical Processes in Soil. In *X-Ray Imaging of the Soil Porous Architecture*; Mooney, S.J., Young, I.M., Heck, R.J., Peth, S., Eds.; Springer: Berlin/Heidelberg, Germany, 2022; pp. 1–229, ISBN 978-3031121760.
39. Scheffler, R.; Neill, C.; Krusche, A.V.; Elsenbeer, H. Soil Hydraulic Response to Land-Use Change Associated with the Recent Soybean Expansion at the Amazon Agricultural Frontier. *Agric. Ecosyst. Environ.* **2011**, *144*, 281–289. [CrossRef]
40. Owuor, S.O.; Butterbach-Bahl, K.; Guzha, A.C.; Jacobs, S.; Merbold, L.; Rufino, M.C.; Pelster, D.E.; Díaz-Pinés, E.; Breuer, L. Conversion of Natural Forest Results in a Significant Degradation of Soil Hydraulic Properties in the Highlands of Kenya. *Soil Tillage Res.* **2018**, *176*, 36–44. [CrossRef]
41. Pinheiro, E.A.R.; de Jong van Lier, Q.; Šimůnek, J. The Role of Soil Hydraulic Properties in Crop Water Use Efficiency: A Process-Based Analysis for Some Brazilian Scenarios. *Agric. Syst.* **2019**, *173*, 364–377. [CrossRef]
42. Matos, A.M.S.; Bonini, C.d.S.B.; Moreira, B.R.d.A.; Andreotti, M.; Heinrichs, R.; Silva, D.T.d.; Souza, J.A.L.d.; Santos, M.A.; Andrighetto, C.; Pavan, G.M.; et al. Long-Term Integrated Crop—Livestock—Forestry Systems Recover the Structural Quality of Ultisol Soil. *Agronomy* **2022**, *12*, 2961. [CrossRef]
43. do Nascimento, D.M.; Cavalieri-Polizeli, K.M.V.; da Silva, A.H.; Favaretto, N.; Parron, L.M. Soil Physical Quality under Long-Term Integrated Agricultural Production Systems. *Soil Tillage Res.* **2019**, *186*, 292–299. [CrossRef]
44. Zhang, Z.; Peng, X. Bio-Tillage: A New Perspective for Sustainable Agriculture. *Soil Tillage Res.* **2021**, *206*, 104844. [CrossRef]
45. Zhang, Z.; Yan, L.; Wang, Y.; Ruan, R.; Xiong, P.; Peng, X. Bio-Tillage Improves Soil Physical Properties and Maize Growth in a Compacted Vertisol by Cover Crops. *Soil Sci. Soc. Am. J.* **2022**, *86*, 324–337. [CrossRef]
46. Moraes, M.T.; Debiasi, H.; Carlesso, R.; Franchini, J.C.; da Silva, V.R.; da Luz, F.B. Age-Hardening Phenomena in an Oxisol from the Subtropical Region of Brazil. *Soil Tillage Res.* **2017**, *170*, 27–37. [CrossRef]
47. De Moraes, M.T.; da Luz, F.B.; Debiasi, H.; Franchini, J.C.; da Silva, V.R. Soil Load Support Capacity Increases with Time without Soil Mobilization as a Result of Age-Hardening Phenomenon. *Soil Tillage Res.* **2019**, *186*, 128–134. [CrossRef]
48. Talukder, R.; Plaza-Bonilla, D.; Cantero-Martínez, C.; Wendroth, O.; Castel, J.L. Soil Gas Diffusivity and Pore Continuity Dynamics under Different Tillage and Crop Sequences in an Irrigated Mediterranean Area. *Soil Tillage Res.* **2022**, *221*, 105409. [CrossRef]
49. Xiong, P.; Zhang, Z.; Guo, Z.; Peng, X. Macropores in a Compacted Soil Impact Maize Growth at the Seedling Stage: Effects of Pore Diameter and Density. *Soil Tillage Res.* **2022**, *220*, 105370. [CrossRef]
50. Landl, M.; Schnepf, A.; Uteau, D.; Peth, S.; Athmann, M.; Kautz, T.; Perkons, U.; Vereecken, H.; Vanderborght, J. Modeling the Impact of Biopores on Root Growth and Root Water Uptake. *Vadose Zone J.* **2019**, *18*, 1–20. [CrossRef]

Disclaimer/Publisher's Note: The statements, opinions and data contained in all publications are solely those of the individual author(s) and contributor(s) and not of MDPI and/or the editor(s). MDPI and/or the editor(s) disclaim responsibility for any injury to people or property resulting from any ideas, methods, instructions or products referred to in the content.